High-frequency spectral decay in P-wave acceleration spectra and source parameters of microearthquakes in southeastern Sicily, Italy

by Giuseppina Tusa[1], Horst Langer[1], Alfonso Brancato[2] and Stefano Gresta[2]

1 *Istituto Nazionale di Geofisica e Vulcanologia – Osservatorio Etneo, Piazza Roma* 2, I-95125 *Catania, Italy. E-mail: giuseppina.tusa@ct.ingv.it*

2 *Dipartimento di Scienze Geologiche, Università di Catania, Corso Italia* 57, I-95129 *Catania, Italy.*

The electronic supplement to this article includes the Tables S1, S2 and S3.

Abstract

In widely used ω^{-2} source models the characteristics of high frequency radiation are described as being flat for frequencies between the source corner frequency and an upper limiting frequency f_{max}. Deviations from this behavior are described in a parameter κ which is understood as a general measure of the changes the signal undergoes on its way from the source to the receiver. In this study, we calculated κ in Southeastern Sicily by using microearthquakes belonging to three different seismic sequences occurring in the area in 1990, 1999-2001, and 2002. The selected events form four different clusters whose seismic sources are located within a 2 km radius. Although the source-to-station paths are approximately the same inside a given cluster, the values of κ change considerably at the same recording site from one event to another, also in the case of events having the same magnitude. We parameterized κ in terms of event (κ^E), and path (κ^P and κ^{Diff}) contributions. The term κ^P represents the contribution on total κ of both the whole source-to-station path and the near-surface geology, while κ^{Diff} models the possible spatial variation in the parameter measured with respect to a reference source-station direction. Results show that the source contribution is not negligible and that there is a positive correlation with source size exists. Moreover, the hypothesis of a laterally homogeneous crustal structure within the area in question is not appropriate and significant variation in attenuating properties of the medium may occur in a very small distance range (also in the order of a few tens of meters). Our analysis suggests that the origin of the above mentioned variability is located near the recording site. Synthetic spectra are also computed in order to verify the actual significance of the parameterization employed and its capacity to separate the source and the path contribution to κ.

We describe our spectra as a product of a Brune-type source spectrum and an exponential shaping term accounting for propagation effects. The seismic moments range between 3.8×10^{11} and 5.2×10^{13} N·m, the source radii range between 176 and 669 m, while the stress drop varies from 0.01 to 0.67 MPa.

Introduction

At high frequencies (greater than corner frequency), the spectral shape of ground acceleration spectra predicted by ω^{-2} standard source model (e.g. Brune, 1970) is generally flat. In order to describe the deviation from a flat high-frequency acceleration spectrum, Anderson and Hough (1984) introduced the spectral decay parameter κ. They proposed that the shape of the acceleration spectrum can be described by

$$A(f) = A_0 e^{-\pi f \kappa} \qquad f > f_E \tag{1}$$

where A_0 depends on source, epicentral distance, and other factors, f_E is the frequency above which the spectral amplitude follows an exponential decay, and κ is the controlling spectral decay parameter, estimated by fitting the trend of a spectrum curve at frequencies above f_E. Anderson and Hough (1984) and Anderson (1986, 1991) suggested that κ describes a degree of attenuation and can be broken down as

$$\kappa(r, S) = \kappa(r) + \kappa(S) \tag{2}$$

where $\kappa(r)$ describes the distance (r) dependence of κ and $\kappa(S)$ is the near-surface attenuation specific to each site S. This model implies that when the acceleration spectra of ground motion can be described by the exponential decay, the spectral shape is not sensitive to the frequency dependence of quality factor, and κ equal to t^* ($=\int_{path} ds/Q\nu$).

Since its introduction, the determination of κ has become important for describing of the intrinsic high-frequency attenuation and many studies are now available on this topic. For example, Boore and Atkinson (1987) and Beresnev and Atkinson (1997) used κ for stochastic prediction of

ground motion. Castro *et al*. (2000) used κ for the analysis of the spatial variation of Q near the seismogenic zone, supporting a propagation path origin of the spectral decay. Conversely, Tsai and Chen (2000) suggested that the high-cut process of strong-motion accelerations results from source and site effects, while distance dependent attenuation is the least important parameter controlling κ. By applying a method based on the technique by Iwata and Irikura (1988), Petukhin and Irikura (2000) proposed that the spectral fall-off is controlled by a source effect. Purvance and Anderson (2003) did not find any statistically significant dependence of κ on epicentral distance and concluded that $\kappa = \kappa^{site} + \kappa^{event}$ is an effective parameterization of κ. Similarly, Bindi *et al*. (2006) evaluated the parameter κ isolating the source, site and propagation contributions by using 245 aftershocks following the 1999 Izmit earthquake. They found that the source contribution is not negligible and κ^{event} shows a positive correlation with magnitude. Moreover, the dependence of κ on distance weakens for distances over about 30 km, and reverses, with slightly decreasing values, for ray paths longer than 80 km. All these studies reveal contradictory results and suggest that there are still unresolved aspect on the origin of high frequency spectral decay.

Investigations into the attenuation parameter κ of local earthquakes in southeastern Sicily were performed by Tusa and Gresta (2008). The authors computed the parameter κ from the slope of the high-frequency part of the P-wave acceleration spectra after correcting for attenuation along the seismic path. They found average κ values between 0.009±0.008 sec and 0.035± 0.023 sec, and within the bounds of variation, the authors concluded that there was not a statistically significant difference from one station to another. However, the scatter of κ-values suggests that κ spread out over a large range of values and its variability could be in part be due to other factors as well, such as the source. In this work, we present a more detailed analysis concerning the values of κ in Southeastern Sicily, parameterizing it in terms of source and propagation effects (attenuation along the source-to-station path and near-surface attenuation). This study represents a further effort to understand the origin of the high-frequency spectral decay in the studied region. We use

microearthquakes belonging to three different sequences occurring in the area in 1990, 1999-2001, and 2002. We evaluate the dependence of κ on the source and path by using a new approach based on the use of clustered events, namely with having hypocentral locations as close as possible to each other. The selected events have been located with high precision relative location (Scarfì *et al*., 2003; Brancato *et al*., 2009) and are thus suitable to investigate the influence of the complexity of the propagation effects on the observed variability of κ. Additionally, we invert the spectra of P body-wave seismograms for corner frequency and low-frequency level by means of a specific inversion procedure which allows the removal of propagation effects from the observed spectra. Thus, the seismic moment, the source dimension, and the stress drop of the selected events were computed in order to both determine scaling laws and investigate possible departures from self-similarity in the studied magnitude range.

The Data

The data we present here concern earthquakes belonging to three different seismic sequences occurring in Southeastern Sicily in December 1990, November 1999 – January 2000, and February – September 2002.

December 1990 Sequence

The studied events occurred during the aftershock activity that followed the December 13, 1990 earthquake (M_L 5.4, 00:24 UTC). The data were recorded by the stations of a portable seismic network that was installed by Istituto Nazionale di Geofisica (now Istituto Nazionale di Geofisica e Vulcanologia) (Fig. 1) two days after the main shock. Four stations were equipped with three-component sensors (two short-period Teledyne S-13 (CIU and TDA) and two broadband Guralp CMG4-T (BCC and MLT)) and five with vertical component (S-13) sensors (Amato *et al*., 1995).

The seismic signals were digitized by a Lennartz 5800 system, with a dynamic range of 120 dB and a sampling rate of 125 samples per second.

The aftershock activity is considered rather low for a magnitude 5.4 main shock in both magnitudes and number. In fact, within two days of the main shock only eight events were recorded having magnitudes between 2.2 and 2.9. Three events (M_{max} 2.6) were the only other ones recorded until a M_L 4.6 event on 16 December (13:50 UTC). The latter was followed by a sequence of aftershocks (M_{max} 3.0) (Amato *et al.*, 1991). On a total of 300 earthquakes detected by the portable network during the aftershock activity, recently Brancato *et al*. (2009) have recently localized 48 well-recorded events (with at least four P-first arrival times). The locations were determined by using the program HYPOELLIPSE (Lahr, 1999) and the 1D velocity model for the Hyblean area by Musumeci *et al*. (2003). On average, the horizontal and vertical errors are 3.7 km and 1.9 km, respectively. Eighteen events of the 48 above mentioned have been relocated with high precision relative location by Brancato *et al.* (2009) who applied the cross-spectral method (Frémont and Malone, 1987). See Brancato *et al*. (2009) for a detailed description of the procedure followed. We only note that the cross-correlation analysis has shown that some earthquakes in the 1990 sequence have very similar waveforms and define a multiplet of closely spaced events.

Brancato *et al.* (2009) calculated a cumulative focal mechanism using the FPFIT algorithm (Reasenberg and Oppenheimer, 1985). They found a normal faulting mechanism with a left-lateral component, on a plane striking 150° ± 8°, dipping 65° ± 8° and with a rake angle of -50° ± 10° (Fig. 2a). This solution is unique, with a misfit of 0.18, and the consistency of the polarities for the different events suggest a homogeneous faulting mechanism for all the aftershocks. Consequently, we consider these fault plane solutions as representative for the whole cluster and use it for the correction of the spectral amplitudes with respect to the radiation pattern.

November 1999 – January 2000 Sequence

In November 1999 and January 2000, two microearthquake swarms were recorded by the stations of the Southeastern Sicily Seismic Network (SESSN, Fig. 1). Each station was equipped with short-period Mark L4-3D seismometers having a natural frequency of 1.5 Hz and a damping of 60 % of critical. The seismic data were sampled at a sample rate of 125 samples per second and transmitted by radio telemetry to the data acquisition center in Catania. The corner frequency of the antialias filter is 51 Hz, and the amplitude resolution was formally 24 bits.

As reported by Scarfì *et al*. (2003), the hypocentral distribution of the events and the comparison of the waveforms clearly indicated that the swarms formed two distinct families of multiplet events, clustered closely together. In particular, Scarfì *et al*. (2003) performed high-precision relative locations following the method by Frémont and Malone (1987). The authors used data from six stations and tested the stability of their relocation by performing a Monte Carlo experiment obtaining an uncertainty of about ± 10 m in longitude and about ± 50 m in latitude and depth. From the relocation, Scarfì *et al*. (2003) detected two tight clusters: the first cluster corresponds to a vertically oriented planar volume with an extent of about 500 m and horizontal dimensions of about 200 m and 80 m; the second one forms a more stocky body with dimensions of about 300 m and 120 m in the NNW-SSE and ENE-WSW directions, respectively, and about 250 m in the vertical direction. Moreover, Scarfì *et al*. (2003) computed the composite fault-plane solution of the two families that we used to correct the spectral amplitude for radiation pattern.

February - September 2002 Sequence

A microearthquake cluster (largest magnitude 3.6) occurred in the Gulf of Catania during 2002. The sequence started on 21 February and stopped on 12 September 2002, with two isolated shocks (M_L 3.6 and 1.9, respectively), while its bulk occurred in May, with eleven earthquakes (M_L 1.3-2.8) on 14 and four additional events during 17-24 May (M_L 1.5-2.7). The events belonging to the swarm were recorded by the digital stations of SESSN (Fig. 1).

From the whole data set, Brancato *et al.* (2009) selected only ten events having at least 4 readable P-first arrival times and computed a cumulative focal mechanism (Fig. 2b) by using the FPFIT algorithm (Reasenberg and Oppenheimer, 1985). The authors found a focal plane solution that suggest a normal faulting mechanism, with a strike of 100°±10°, a dip of 60°±5°, and a rake of -120°±5°. Moreover, Brancato *et al.* (2009) applied the cross-correlation analysis to the same events by using the data from the stations SR3, SR5, and SR9 and concluded that all ten events in the swarm form a single multiplet. Finally, the precise relative locations for the events suggested that the swarm was aligned along a NE-SW structure, supporting the result obtained from the composite focal plane solution, at a focal depth ranging between 14 and 17 km. The estimated focal mechanism was used to correct spectral amplitudes for effects of the radiation pattern.

Data Selection and Analysis

Based on the results coming from high-precision relative locations of the above described three seismic sequences, for each of them we selected only the events located within a distance of 2 km from each other. Thus, we can investigate source-station paths having approximately the same distance and azimuth. A starting data set of 53 events was obtained: i) six events belonging to the December 1990 sequence (hereinafter indicated as "CL1"); ii) all the events belonging to the November 1999 – January 2000 sequence (hereinafter indicated as "CL2a" and "CL2b" for the first and the second family, respectively); iii) five events belonging to the February-September 2002 sequence (hereinafter indicated as "CL3").

For the cluster 1990, we used only the recordings collected by the stations AUG, CIU, CRN, MSV and TDA, since the remaining ones had poor quality records (Table S1 in the electronic supplement to this article). For the same reason we excluded the recordings collected by the station SR8 of the SESSN (Table S2 in "in the electronic supplement to this article"). On the whole, the

analyzed events have magnitudes M_L, from 1 to 2.9, hypocentral distances ranging between ~20 and 75 km, and focal depth of 13-21 km.

For each event, we calculated the Fast Fourier transform of the P-wave signal on the vertical components using a 1.024-s time window that starts 0.1 s before P-wave arrival. The time windows were tapered with a 10% cosine taper at the beginning and end of the series. Additionally, we estimated the noise level by calculating the spectra of the pre-event noise in the same manner as for the signal. As a first step, recordings with signal-to-noise ratios lower than 2 for frequency in the range ~2 ÷ 25 Hz, for cluster CL1, and from ~2 to 30 Hz, for the remaining clusters, were removed from the analysis. Then, the spectra of the selected recordings were corrected for instrumental response and transformed to acceleration spectra, multiplying the amplitudes by ω. In order to determine the frequency interval beyond the corner frequency, f_c, where the high-frequency spectral decays are independent of the source, we first separated the source and propagation effects from the spectral records of the selected events. In particular, the observed spectrum $A_{ij}(f,R)$ from event i recorded at site j can be represented by the following model:

$$A_{ij}(f,R) = R_{\theta,\varphi} S_i(f) G(R) P_{ij}(f,R) \tag{3}$$

where f is the frequency, R is the hypocentral distance, $R_{\theta,\phi}$ is the source radiation pattern, that has been computed on the basis of available fault-plane solutions (Scarfì *et al*., 2003; Brancato *et al*., 2009), $S_i(f)$ is the acceleration source function of event i, $G(R)$ is the geometrical spreading, and $P_{ij}(f,R)$ is a propagation function that we assume to represent the anelastic attenuation and the site effect near the j-th station. Since 83% of hypocentral distance values are less than 50 km (96% are less than 55 km), we approximated the geometrical spreading $G(R)$ with $1/R$. Additionally, we normalized the spectral amplitude at a distance R′=30 km. A system of linear equations can be set rewriting (3) as:

$$Log\left[R_{\theta,\varphi}^{-1}A_{i,j}(f,R)R/R'\right]=LogS_i(f)+LogP_{i,j}(f,R) \tag{4}$$

In matrix form this can be represented as

$$\begin{bmatrix} b_{i1} \\ b_{i2} \\ \vdots \\ b_{ij} \end{bmatrix} = \begin{bmatrix} 1 & 1 & 0 & \cdots & 0 \\ 1 & 0 & 1 & \cdots & 0 \\ \vdots & \vdots & \vdots & \vdots & \vdots \\ 1 & 0 & 0 & \cdots & 1 \end{bmatrix} \cdot \begin{bmatrix} s_i \\ p_{i1} \\ p_{i2} \\ \vdots \\ p_{ij} \end{bmatrix} \tag{5}$$

where $b_{ij}=Log\left[R_{\theta,\varphi}^{-1}A_{i,j}(f,R)R/R'\right]$, $s_i=LogS_i(f)$, $p_{ij}=LogP_{i,j}(f,R)$. For simplicity equation (5) may be expressed as

$$\boldsymbol{b} = \boldsymbol{A}\boldsymbol{x} \tag{6}$$

where $\boldsymbol{b}$ is the data vector (spectral values at a given frequency), x denotes the model vector (spectral value at the same frequency for the source spectrum), and $\boldsymbol{A}$ is a matrix with J rows and J+1 columns that relates $\boldsymbol{x}$ to $\boldsymbol{b}$. For a given event, recorded at J stations, there are K(=1×J) equations to determine the 1+J unknown parameters for each frequency. We solved the matrix equation by using the singular value decomposition, SVD (Lawson and Hanson, 1974) of A given by $A=U\Lambda V^T$, to determine the minimal norm least squares solution to (6). In our inversion scheme, the source and propagation terms are determined separately at each frequency. Among the 53 events comprised in our starting data set, we selected only those for which at least three acceleration spectra were available. A total of 29 events were considered suitable for the application of the above explained procedure (see Fig. 3).

The acceleration source spectra can be modeled by (Boatwright, 1978)

$$\Omega(f) = \frac{\Omega_0 (2\pi f)^2}{\left[1 + \left(\frac{f}{f_c}\right)^{n\gamma}\right]^{1/\gamma}} \tag{7}$$

where Ω_0 is the low-frequency spectral level, f_c is the corner frequency, and n and γ are dependent on the source model and define the high-frequency decay at the source. For $n = 2$ and $\gamma = 1$, $\Omega(f)$ is equivalent to the Brune ω^{-2} source model (Brune 1970, 1971). To avoid problems associated with the visual determinations of spectral parameters and to minimize the difference between theoretical and inverted acceleration source spectra (s_i in eq.(5)), a best-fitting search algorithm was used (Tusa *et al*., 2006a, b) We modified here the misfit function as follows (Parolai *et al*., 2007)

$$\varepsilon = \sqrt{\frac{\sum_{m=f_{\min}}^{f_{\max}} (Log\Omega_{ob}(f_m) - Log\Omega_{th}(f_m))^2}{N}} \tag{8}$$

where f_{min} and f_{max} define the working frequency band permitted by the data, $\Omega_{ob}(f_m)$ and $\Omega_{th}(f_m)$ are the observed and theoretical amplitude spectra at the mth frequency, respectively, and N is the number of frequencies in the frequency band $f_{min} \div f_{max}$ (1.95 ÷ 25 Hz for cluster 1990, and 1.95 ÷ 30 Hz for the remaining ones). When a minimum of the misfit function is found, the computed values are accepted as the best estimated spectral parameters. We run the inversion procedure using differing source models to find the best fit. In particular, four source models were tested: the Brune (1970, 1971) ω^{-2} spectrum (n=2 and $\gamma = 1$), the Boatwright (1978) ω^{-2} spectrum (n=2 and $\gamma = 2$), the Brune ω^{-n} spectrum (n variable and γ=1), and the Boatwright ω^{-n} spectrum (n variable and γ=2). In order to prevent trade-off between the model parameters Ω_0, f_c, and n for each of the spectra and to provide some stability to the model, we initially determine the starting model parameters by

visually fitting the inverted acceleration source spectra (s_i). The inversion was carried out trying various initial guesses. In general we fixed Ω_0 in a first stage and allowed f_c and n to vary. We then adjusted Ω_0 and n by fixing f_c at the value obtained during the first stage. In a further step we used the n value for the model with the best misfit obtained so far and inverted just for Ω_0 and f_c. We selected the best Ω_0, f_c, and n values which will represent the new starting model. The procedure is started over again until the misfit function indicates no further improvement of the results. Table 1 summarizes the results of inversion procedures in terms of minimum, maximum and mean values of misfit function obtained for the different source spectral models. The best-fitting source model was found to be the Brune ω^{-n} spectrum which, except for one case, always produced a significant reduction of the misfit and was therefore considered the most suitable to describe this dataset (see Fig. 4).

We found that the high-frequency spectral decay (n) of the source spectra is, in general, higher than that prefigures by ω^{-2} model ($2.1 \leq n \leq 3.$, with values higher than 2.5 in 80% of the cases) suggesting that an ω^{-2} model is not sufficient to describe completely the high-frequency part of the source spectra of the considered events (e.g., Parolai *et al.*, 2007). In this respect, the deviation from ω^{-2} model can be accounted for by the function (Halldorsson and Papageorgiou, 2005)

$$D(f,\kappa) = \exp(-\pi f \kappa) \tag{9}$$

where κ defines the source contribution (κ_{event} by Purvance and Anderson, 2003) in characterizing the high-frequency source spectral decay. In order to resolve the trade-off between κ and f_c, we obtain independent values of κ by using a new approach described below. We estimate f_c values below 11 Hz, whereas κ is obtained considering frequencies above 15 Hz and in particular 15 ÷ 25 Hz for cluster CL1, and of 15 ÷ 30 Hz for the other clusters.

Source and path contribution on κ: formulation of the method

Following Purvance and Anderson (2003), κ for the *i*th earthquake at the *j*th station can be parameterized as follows:

$$\kappa_{ij} = \kappa_i^E + \kappa_j^S + \kappa_{ij}^D \tag{10}$$

where κ_i^E and κ_j^S are the parameters of the model that describe the dependence of κ on the source of the earthquake and of a specific recording site, respectively, while κ_{ij}^D represents the dependence of κ on distance of the event *i* for station *j*. In detail, κ^E depends on source characteristics, varying with focal mechanism (Purvance and Anderson, 2003), and shows a positive correlation with magnitude (Purvance and Anderson, 2003; Bindi *et al.*, 2006). κ^S is considered as a measure of the attenuation through the shallow crustal layers, and is reported as being generally smaller for sites on rock than for sites on soft sediments. Finally, κ^D is considered as a measure of whole path propagation effects. Bindi *et al.*, 2006 found an increase of κ^D with distance. Before computing κ_{ij}, the acceleration spectra of the selected recordings, corrected for instrument response, are smoothed with a 2 Hz moving average window. Thus, we estimated the slope of the high frequency decay of the acceleration spectrum above 15 Hz, plotted in a semilogarithmic diagram (see Fig.5), by a linear least-squares regression in the above mentioned frequency ranges. Table 2 gives the estimated values of κ_{ij} and the standard deviation (SD) resulting from the linear fit. κ_{ij} shows a great variability of values (from 0.0034 to 0.0871 s), while, on the whole, the standard deviation (SD) is less than 50% in 80% of the cases. These low values of SD correspond to the considerable goodness of the linear fit of the high-frequency spectral amplitude decay shown in Figure 5.

Exploring the values of κ_{ij} inside the same cluster, it appears evident that κ_{ij} can change considerably at the same recording site from one event to another. As an example in Figure 5 we show some acceleration spectra together with the estimates of κ_{ij} obtained at the stations CIU (for CL1), SR1 (for CL2a), and SR4 (for CL3). For instance, the values of κ_{ij} for the events #9006 and #9009 (cluster CL1) at station CIU are 0.0871±0.0049 and 0.0348±0.0059, respectively. Since at a given station we cannot ascribe the differences in the κ_{ij} to a variation in the material properties, the source properties and/or the whole path attenuation thus affect the estimates of κ_{ij}. In the attempt to explain the observations, it should be noted that the frequency range used for evaluating κ_{ij} does not include the corner frequency of the considered events which could affect the slope of the spectrum decay. In this way we minimized the corner frequency contamination. We can also exclude the focal mechanism as a factor responsible for the observed differences, since the events share the same one (Brancato *et al.*, 2009). However, if this were not true and there is some difference in the focal mechanisms of the two considered events, the variability of κ_{ij} should be present at the other stations, as well, which in our case was not observed (see Table 2). Additionally, even if this eventuality is not entirely certain, the characteristic similarity of waveforms of multiplet events over long time windows makes differences in focal mechanisms rather unlikely. If the observations were due to the M_L, the variability of κ_{ij} should still be found at all stations, and events with comparable M_L should have comparable κ_{ij} (for example events #3 and #13 at SR1). This is not shown both in Figure 5 and Table 2. Conversely, we could ascribe the variability of κ_{ij} to a difference in the stress drop values that can vary from one source to another even if their M_L is similar. Indeed, sources with higher stress drop values may generate higher high-frequency energy content, which produce smaller κ_{ij}.

In the attempt to explain the observations also as a wave propagation effect, it should be noted that inside a given cluster the distances between events may be considered negligible (being on the whole ≤ 2 km) and the same source-to-station path and the same azimuth can be assumed.

Under this condition, we expect that acceleration spectra related to two sources located along the same azimuth, recorded at the same station, characterized by the nearly coincident near-station propagation path and same magnitude have comparable frequency content. However, if the events show different frequency content, we cannot exclude that there are spatial variations in the attenuation structure along the path from the source to station and that a significant complexity of the wave propagation effects affect the spectral shape at high frequency. We therefore modify the equation (10) as follows:

$$\kappa_{ij} = \kappa_i^E + \kappa_j^P + \kappa_{ij}^{Diff} \tag{11}$$

where κ_j^P represents the contribution on κ_{ij} of the whole path from the hypocenter to the *j*-th recording site and includes the contribution of the near-surface geology on total κ, as well. It will be assumed as identical for all the events within a given cluster. Then, taking into account the minimum value of κ_{ij} at each station as reference value (for the corresponding event we have κ_{ij}^{Diff} equal to 0), κ_{ij}^{Diff} will represent the possible changes of κ not explained by κ_i^E and κ_j^P. A system of linear equations is obtained from equation (11) by taking into account all the κ_{ij} estimated for all the earthquakes belonging to a given cluster. In matrix form this system of equations can be written as

$$\begin{bmatrix} \kappa_{11} \\ \kappa_{21} \\ \vdots \\ \kappa_{i1} \\ \kappa_{12} \\ \kappa_{22} \\ \vdots \\ \kappa_{i2} \\ \vdots \\ \kappa_{1j} \\ \kappa_{2j} \\ \vdots \\ \kappa_{ij} \end{bmatrix} = \begin{bmatrix} 1 & 1 & 0 & 0 & 0 & \cdots & 0 & 0 & 0 & 0 & \cdots & 0 & \cdots & 0 & 0 & 0 \\ 0 & 1 & 1 & 1 & 0 & \cdots & 0 & 0 & 0 & 0 & \cdots & 0 & \cdots & 0 & 0 & 0 \\ \vdots & \vdots & \vdots & \vdots & \vdots & \vdots & \vdots & \vdots & \vdots & \vdots & \vdots & \vdots & \vdots & \vdots & \vdots & \vdots \\ 0 & 1 & 0 & 0 & 0 & \cdots & 1 & 1 & 0 & 0 & \cdots & 0 & \cdots & 0 & 0 & 0 \\ 1 & 0 & 0 & 0 & 0 & \cdots & 0 & 0 & 1 & 0 & \cdots & 0 & \cdots & 0 & 0 & 0 \\ 0 & 0 & 1 & 0 & 0 & \cdots & 0 & 0 & 1 & 1 & \cdots & 0 & \cdots & 0 & 0 & 0 \\ \vdots & \vdots & \vdots & \vdots & \vdots & \vdots & \vdots & \vdots & \vdots & \vdots & \vdots & \vdots & \vdots & \vdots & \vdots & \vdots \\ 0 & 0 & 0 & 0 & 0 & \cdots & 1 & 0 & 1 & 0 & \cdots & 1 & \cdots & 0 & 0 & 0 \\ \vdots & \vdots & \vdots & \vdots & \vdots & \vdots & \vdots & \vdots & \vdots & \vdots & \vdots & \vdots & \vdots & \vdots & \vdots & \vdots \\ \vdots & \vdots & \vdots & \vdots & \vdots & \vdots & \vdots & \vdots & \vdots & \vdots & \vdots & \vdots & \vdots & \vdots & \vdots & \vdots \\ 1 & 0 & 0 & 0 & 0 & \cdots & 0 & 0 & 0 & 0 & \cdots & 0 & \cdots & 1 & 0 & 0 \\ 0 & 0 & 1 & 0 & 0 & \cdots & 0 & 0 & 0 & 0 & \cdots & 0 & \cdots & 1 & 1 & 0 \\ \vdots & \vdots & \vdots & \vdots & \vdots & \vdots & \vdots & \vdots & \vdots & \vdots & \vdots & \vdots & \vdots & \vdots & \vdots & \vdots \\ 0 & 0 & 0 & 0 & 0 & \cdots & 1 & 0 & 0 & 0 & \cdots & 0 & \cdots & 1 & 0 & 1 \end{bmatrix} \cdot \begin{bmatrix} \kappa_1^E \\ \kappa_1^P \\ \kappa_2^E \\ \kappa_{21}^{Diff} \\ \vdots \\ \kappa_i^E \\ \kappa_{i1}^{Diff} \\ \kappa_2^P \\ \kappa_{22}^{Diff} \\ \vdots \\ \kappa_{i2}^{Diff} \\ \vdots \\ \kappa_j^P \\ \kappa_{2j}^{Diff} \\ \vdots \\ \kappa_{ij}^{Diff} \end{bmatrix} \qquad (12)$$

Here the matrix A depends on the source-to-station geometry. We solved the matrix equation by still using the singular value decomposition, SVD (Lawson and Hanson, 1974). Only the κ_{ij} values with SD<50% have been used to evaluate the source and path contribution on the spectral decay parameter. The same SVD technique is also used to compute the associated uncertainty to each of the terms given in the second member of equation (11). To do this we solved the system of equations by considering the values of $\kappa_{ij} \pm$ SD, as well. The differences between the values of the different terms (κ_i^E, κ_j^P and κ_{ij}^{Diff}) obtained considering κ_{ij} with those obtained considering $\kappa_{ij} \pm$ SD give us the associated uncertainties.

Results

Table 3 lists the values of κ^E obtained for 21 earthquakes from our inversion scheme. The absent values are the ones relative to the events for which only a datum was available and hence not

enough to constrain κ^E. The κ^E term ranges from -0.0008 ± 0.0013 s to 0.0253 ± 0.0054 s, and plotted against the local magnitude (Fig. 6a) shows a positive linear correlation with it. The equation of the best-fit line of the results in Figure 6a is κ^E=0.0088M_L–0.0069 with a coefficient of correlation equal to 0.53. Performing a Student's *t* test we rejected the null hypothesis "no correlation between κ^E and M_L" at the 1% significance level. The contribution of path effect on the measured decay parameters is shown in Figure 6b, where we plot κ^P as a function of hypocentral distance for all the station sites as obtained for each of the four clusters. The values of κ^P for those stations that we only had one value of total κ (for instance AUG for CL1 or SR5, SR6, and SR7 for CL3) have not been included. In exploring the behavior of κ^P with distance, we should point out that κ^P represents the effect of the whole propagation path from source to receiver, thus it can be interpreted as the sum of terms κ_j^S and κ_{ij}^D of equation (10). κ^P values display noticeable variability between 0.0011 ± 0.0011 and 0.0308±0.0026, and must be interpreted as being associated to varying whole path attenuation effects. However, if a dependence of total κ on distance exists, different values of κ^P encountered at similar hypocentral distances have to be attributed to near-surface attenuation under a receiver site. Vice versa, comparing the κ^P values obtained for the same station site, but computed from the different clusters, it is possible to investigate distance dependence of the decay parameter. The values of κ^P obtained for the stations SR2 and SR3 from data of the different clusters, indeed seem to suggest a tendency of increasing with distance of κ^P. Finally, the term κ^{Diff} varies in the range of -0.0120±0.0014÷0.0380±0.0011, and for a given station site it can change markedly from one event to another inside a cluster (Table 4). The large variability shown by κ^{Diff} was expected from the complex behavior of total κ previously described. In this context, the negative values of κ^{Diff} will indicate that along a given source-to-station path an effect able to produce an increase of high-frequency energy in the analyzed frequency band is acting, predominating over the ones which produce a decrease, with respect to the path of reference

(the path related to minimum κ_{ij} value). A potential effect responsible for the variability shown by κ^{Diff}, that we cannot a priori exclude, is a differing rupture directivity of the sources belonging to the same cluster. The rupture directivity produces an azimuthal dependence of seismic first-pulse shape, with higher amplitudes and shorter durations for stations located at an azimuth of the rupture propagation. Unfortunately, we do not have sufficient station coverage to investigate this effect. However, if we suppose that at a given station κ^{Diff} changes from one event to another, into the same cluster, because the associated sources are directive in a different way (e.g. different slip direction along the surface rupture), thus the pulse widths will systematically change with κ^{Diff}. To test possible variations of κ^{Diff} due to differing directivity of sources, we performed a simple analysis measuring the P-wave velocity pulse widths of the events available for station CIU. We selected this station for two reasons. First, it is the station showing the largest variability in the κ^{Diff} values. Second, even if station MSV has the same number of κ^{Diff} estimates as CIU, this last station is characterized by smaller values of hypocentral distances. Indeed, at long distances from a given source (of course not rupturing vertically), the directivity effects can be masked by noise from interference of other seismic phases (multipath phases included), attenuation, resonance, site response and others. We find that the initial P-wave pulse widths (first break to first zero crossing) and the height of the pulses as well are clearly related to the size of the event, and no systematic change with κ^{Diff} can be highlighted. Then, we conclude that the large variability shown by κ^{Diff} is due to the propagation effects, able to influence the high-frequency energy content in the analyzed frequency band, producing attenuation or amplification with respect to the path of reference.

Synthetic data

Working with synthetic data offers the possibility to reproduce the observations arising from real data with the advantage that input parameters are known. In our case, the synthetic tests help us

verify the actual significance of the parameterization employed and its capacity to separate the source and the path contribution on κ. A synthetic database has been created by considering a single layer overlying bedrock and modeling the acceleration spectrum *W(f,R)* recorded at a distance *R* using

$$W(f,R) = \Omega_0 \frac{(2\pi f)^2}{1+\left(\frac{f}{f_c}\right)^{2+b}} \frac{1}{R} e^{-\pi f \kappa_h} |Z(f)| + noise(f) \tag{13}$$

where *noise(f)* is a white noise different in each simulation, κ_h is the term that describes the propagation effect in the half-space (see Table 5), and *b* is an additional factor that simulates the source contribution to κ in increasing the high-frequency source spectral decay with respect to ω^{-2}-model. *Z(f)* is the site term. For the sake of simplicity we described it by using the formula of Safak (1995) for 1D analytical transfer function given by

$$|Z(f)| = \frac{\left[(1+s)^2 + 1/16Q_2^{\,2}\right] e^{-2\pi f k_{site}}}{\left\{1+2\left[s\cos(4\pi ft) - 1/4Q_2 \sin(4\pi ft)\right] e^{-2\pi f k_{site}} + (s^2 + 1/16Q_2^{\,2}) e^{-4\pi f k_{site}}\right\}} \tag{14}$$

where Q_2 is the quality factor of the soil layer. Let indicate with V_1 and ρ_1 the velocity and density of the bedrock, and with V_2 and ρ_2 the velocity and density of the overhanging soil layer (having thickness d_2). Thus, in equation (14) *s* is the reflection coefficient related to the impedance contrast *c*:

$$s = \frac{\rho_1 V_1 - \rho_2 V_2}{\rho_1 V_1 + \rho_2 V_2} = \frac{c-1}{1+c} \tag{15}$$

Moreover, the following relationships between the several parameters are used

$$d_2 = \frac{V_2}{4 f_0}; \quad t = \frac{d_2}{V_2}; \quad \kappa_{site} = \frac{t}{Q} \tag{16}$$

where f_0 is the fundamental resonance frequency of the site response, t is the travel time through the soil-layer, and κ_{site} describes the contribution of the near-surface attenuation on total κ. Concerning the source properties, we assume a Brune source model and the following relationships are then considered:

$$\Omega_0 = \frac{2 R_P M_0}{4 \pi V^3 \rho}; \quad r_S = \sqrt[3]{\frac{7 M_0}{16 \Delta\sigma}}; \quad f_c = 2.34 \frac{V}{2 \pi r_S} \tag{17}$$

where M_0 is the seismic moment, $\Delta\sigma$ is the stress drop, R_P is the P-wave average radiation pattern, V and ρ are the P-wave velocity and density in the half-space, respectively, r_S is the source radius, and f_c is the corner frequency.

Three different terms determine the high-frequency decay of the synthetic spectrum *W(f,R)*: κ_h in the half-space, κ_{site} and κ_{event}. Therefore, it follows that κ_{tot} numerically estimated fitting a straight line to the logarithm of the acceleration spectrum *W(f,R)*, is given by

$$\kappa_{tot} = \kappa_{event} + \kappa_h + \kappa_{site} \tag{18}$$

The synthetic spectra are generated for a cluster of five co-located events, recorded at 3 different sites (S_1, S_2, and S_3) having epicentral distance of 30 km. We hypothesize that the values of κ_h in the half space are 0.04 s along the source-to-S_1 path, 0.03 s along the source-to-S_2 path, and

0.02 s along the source-to-S_3 path. We also hypothesize that the velocity V_2 in the soil-layer changes from one event to another (see Table 5), which means assuming different resonance frequency f_0 (varying between 1.5 and 4.5 Hz). In this way we simulate a laterally heterogeneous crustal structure able to produce a different propagation effect contribution on the value of κ_{tot}. Summarizing, all the synthetic spectra share the same κ_h for a given source-to-site path, while κ_{site} and κ_{event} are different.

For each simulation, we perform the least-square fit for frequency higher than 15 Hz, since the corner frequency of simulated spectra ranges from 4 to 13 Hz. First, the estimated κ (hereinafter κ_{totE}) is compared with the imposed one (κ_{tot}) by determining the error $\varepsilon = [(|\kappa_{tot} - \kappa_{totE}| / \kappa_{tot}) \cdot 100]$ (see Fig. 7). The value of κ_{tot} is fairly well estimated with error that are $\leq 25\%$, with the exception of event 1 at site S_1 ($\varepsilon = 45\%$) that we exclude from successive calculations (extreme conditions for model parameters). The minimum value of κ_{totE} at each site is the reference value given by

$$\kappa_{totEMin} = \kappa_{event} + \kappa_h + \kappa_{site} = \kappa_{event} + \kappa_P \tag{19}$$

where κ_P expresses the contribution of the whole path source-to-site on κ_{totE}. In light of this, the other κ_{totE} values at the same site are given by

$$\kappa_{totE} = \kappa_{event} + \kappa_P + \kappa_{Diff} \tag{20}$$

where, similarly to the real data, κ_{Diff} represents the effect of a laterally heterogeneous medium. Therefore, we invert the values of κ_{totE} obtained for synthetic data using the method applied for the real data (i.e. constructing the matrices in equation (12) and applying the SVD). Figure 8 shows the comparison between the input (true) and inverted (estimated) values of the κ_{event}, κ_P, and κ_{Diff}. The synthetics show that we predict the input values with an error ε of 25% on average and 67% in the

worst case. On the whole, the Figure 8 demonstrates the ability of the inversion procedure to correctly reconstruct the model parameters with good accuracy. For instance, the increase of κ_{event} with M_L as well as the variation of κ_P for the different source-to site paths, are well-predicted. The same holds for κ_{Diff}, whose values are closely related to the supposed heterogeneity of the attenuation characteristics of the shallowest layer. However, we note that some terms such as the κ_E for events 4 and 5 (κ_{E4} and κ_{E5} in Fig. 8) are significantly underestimated (ε equal to 50% and 48%, respectively), leading to an overestimation of some other terms κ_{Diff} for event 4 and 5 and sites S1 and S3 (referred to as κ_{Diff}^{4S1}, κ_{Diff}^{5S1}, or κ_{Diff}^{5S3} in Fig. 8). In interpreting this result, we have to take into account that the estimated decay parameter κ_{totE} includes a noise term, which obviously causes a scatter of κ_{totE} (the latter used to perform the inversion). In our synthetic experiment we estimated κ_{totE} with uncertainties of 5% (best case) to 33% (worst case). Consequently, the entity of the trade-off reported above is inside the uncertainty. Finally, we performed an ANOVA one-way analysis to test the null hypothesis "significant difference between the true κ-parameters and estimated ones": it can be rejected at 5% of significance level (F = 0.017 vs. a critical value of $F_{1,36,5\%} = 4.11$).

Source parameters

The estimated κ^E terms have been used to account for the source contribution on the high frequency decay of the source spectra by applying the diminution function $D(f,\kappa)$ from 15 Hz, which is the frequency where we began to measure the parameter κ_{ij}. Then the acceleration source spectrum of each event was fit to ω^{-2} model and the corrected spectral parameters were used to estimate seismic moment (M_0), Brune's source radius (r) and static stress drop ($\Delta\sigma$) defined as follow, respectively

$$M_0 = \frac{4\pi\rho R v_p^3 \Omega_0}{R_p} \tag{21}$$

$$r = \frac{\boldsymbol{2.34}\alpha}{\boldsymbol{2}\pi f_c} \tag{22}$$

$$\Delta\sigma = \frac{\boldsymbol{7}}{\boldsymbol{16}} \frac{M_{\boldsymbol{0}}}{r^{\boldsymbol{3}}} \tag{23}$$

where ρ is the density of the medium (2.7 g/cm^3), R=30 km, v_P is the overall average P-wave velocity (average of the all average P-wave velocity computed for each event by using the hypocentral distance and the travel time of the considered seismic phase), R_P is the average radiation pattern for P-waves (0.44), f_c is the corner frequency, α is the *P*-wave velocity near the source (extracted from the 1D-velocity model of Musumeci *et al*. (2003) accounting for the focal depth of the cluster). Note that the events belonging to a given cluster share the same focal depth. The seismic moment (M_0) ranges from 3.8 $\times 10^{11}$ N·m to 5.2 $\times 10^{13}$ N·m, source radius (r) from 176 to 669 m and stress drop ($\Delta\sigma$) varies from 0.007 to 0.67 MPa. The relation between seismic moment and source radius is shown in Figure 9, coupled with contours of constant stress drop from 0.1 to 10 bars. The results suggest a dependence of the seismic moment on source radius. No tendency to deviate from a constant stress-drop scaling can be observed over the magnitude range considered. Finally, in Figure 9 we also plot the average values of M_0 and r obtained by Tusa *et al*. (2006b) for the events 3, 5, 8, 13, 16, and 49 belonging to the November 1999 – January 2000 seismic sequence. Taking into account the uncertainty of the estimates, we can conclude that results are in good agreement with each other.

Discussions and Conclusions

The spectral amplitudes at frequencies higher than 15 Hz have been analyzed by estimating the high-frequency decay parameter κ for microearthquakes belonging to four different clusters of events. The events of a given cluster are located at a distance ≤ 2 km from each other. The estimated values of overall κ'*s* range between 0.0034 and 0.0871 and display noticeable differences both from one station to another inside a given cluster and from one cluster to another at a given station.

Following Purvance and Anderson (2003), we evaluated the dependence on seismic source of observed total κ introducing the term κ^E. We found that κ^E correlates positively with the size of the simulated event, here expressed by means of the magnitude M_L. This result supports the evidence reported by the studies by Purvance and Anderson (2003) and Bindi *et al*. (2006, 2007). Purvance and Anderson (2003) also found a variation of κ^E with focal mechanism which could not be confirmed here. Almost all the events we considered are normal faulting events. Considering the uncertainty associated to κ^E of these events (see Table 3), the values reported by Purvance and Anderson (2003) for the same typology of faulting mechanism are generally smaller than ours, even though still within the bandwidth of our estimations.

The contribution of the complexity of the wave propagation effects on the measured decay parameter has been investigated here through the terms κ^P and κ^{Diff}. We globally estimated a term κ^P ranging from 0.0011±0.0011 to 0.0308±0.0026. Taking into account the stations belonging to the SESSN, we can compare them with the results obtained by Tusa and Gresta (2008) for the studied area. These authors found average $\kappa(r,S)$-values from 0.009±0.008 to 0.024±0.018, which seem to be consistent with the results of the present study (from 0.0011 ± 0.0011 to 0.0245±0.0026 for the station of the SESSN). Since Tusa and Gresta (2008) estimated $\kappa(r,S)$ from the acceleration spectra after correcting for attenuation along the path, the coherency with our κ^P would suggest that the near-surface attenuation rather than the whole path attenuation affects the κ^P values. Moreover, plotting $\kappa(r,S)$ as a function of epicentral distance, Tusa and Gresta (2008) found no dependence on

the distance of κ for all the stations. This seems to contrast with the findings of this study. Indeed Figure 6b seems to show a tendency of κ^P to increase with distance (see stations SR2, SR3 and SR9). However, it is important to recall that, for the same recording site, our κ^P terms can change from a cluster to another since the clusters do not have the same azimuth and spatial variations in structure of the propagating medium are possible.

Let us consider the total κ values estimated for two events, belonging to the same cluster, at two recording sites characterized by approximately the same hypocentral distance from the events. A good example is offered by the events 9006 and 9009 at stations CIU and CRN (see Table 4). Since the distant-dependent terms can be considered approximately the same, we expected that the differences between the total decay parameters at CIU and CRN satisfy the following relation

$$\kappa_{CIU}^{9006} - \kappa_{CRN}^{9006} = \kappa_{CIU}^{9009} - \kappa_{CRN}^{9009} = \kappa_{CIU}^{Site} - \kappa_{CRN}^{Site} \tag{24}$$

From the values shown in Table 2, we see that our results did not support such evidence. A possible interpretation is that the shallow structure of the Earth's crust in southeastern Sicily is laterally heterogeneous and the term κ^P alone is not able to explain the observed variability of our total κ. κ^{Diff} inserts in this context and represents a term to model the possible variation of attenuation parameter measured with respect to a reference source-station direction, for which we put κ^{Diff}=0.

As listed in Table 4, considerable changes of κ^{Diff} are quite common even though the events are located in a very short distance range (ointhe order of a few tens of meters). Its variability does not depend on the relative distance from the hypocenter of the reference event. Similarly, we do not observe a correlation of κ^{Diff} with distance along the source-station paths (κ^{Diff} is not higher for longer travel paths), excluding a possible effect of a higher average source-station attenuation. Moreover, for several events we observe that while the κ^{Diff} is small at one site, at other sites the κ^{Diff} is larger (see the event 13 of CL2a at SR3 (R=41.7 km) and SR1 (R= 28.9 km)). This suggests

that complex wave propagation effects rather than source characteristics govern the shape of the acceleration spectra at high frequency. We are not sure where the observed variation of κ^{Diff} takes place (near rupture area, near the site or along the source-to-station path). However, taking the sum of the terms κ^{P} and κ^{Diff} for each event, an average of the total contribution of the path effects on the spectral decay parameter for each station ($\langle \kappa^{P} + \kappa^{Diff} \rangle$) can be estimated (Table S3, in the electronic supplement to this article). The comparison between κ^{Diff} and $\langle \kappa^{P} + \kappa^{Diff} \rangle$, shows that the highest absolute values of κ^{Diff} characterize the stations with the highest $\langle \kappa^{P} + \kappa^{Diff} \rangle$ (CIU, MSV, SR4), suggesting an origin "near-recording site" for κ^{Diff}. Moreover, the values of $\langle \kappa^{P} + \kappa^{Diff} \rangle$ are consistent with the κ by Tusa and Gresta (2008) and have a tendency to vary with the near-surface site geology. Indeed, the stations situated on volcanic products show higher rates of spectral decay.

The inversion of the synthetic dataset, led us to conclude that parameterization employed is able to correctly separate the source and the path contribution on κ and that the size of the potential trade-offs between the several κ-terms falls inside the uncertainties that characterized the used parameters.

Finally, the acceleration source spectra fitted by considering the ω^{-2} model and the high-frequency diminution function (Halldorsson and Papageorgiou, 2005) have been used to estimate source parameters. The scaling of the seismic moment with source radius is plotted in Figure 9, where the results by Tusa *et al*. (2006b) for common events are reported, as well. In the investigated seismic moment range – which is rather small – we cannot identify a dependency of stress drop on seismic moment, i.e. we have no indications for a breakdown of self-similarity scaling laws. For eight events, the comparison with the value of source parameters obtained by Tusa *et al*. (2006b) suggests that, within the bounds of uncertainty, the results are in a good agreement with each other.

Data and Resources

Seismograms used in this study are not accessible to the public.

Acknowledgments

Research supports from University of Catania, Fondi di Ateneo 2008

References

Amato, A., R. Azzara, A. Basili, C. Chiarabba, M. Cocco, M. Di Bona, and G. Selvaggi (1991). La sequenza sismica del dicembre 1990 nella Sicilia orientale: analisi dei dati sismometrici, *Publ. Ist. Naz. Geofis.* Roma **537**, 57-83 (in Italian).

Amato, A., R. Azzara, A. Basili, C. Chiarabba, M. Cocco, M. Di Bona M., and G. Selvaggi (1995). Main shock and aftershocks of the December 13, 1990, eastern Sicily earthquake, *Ann. Geofis.* **38**, 255–266.

Anderson, J. G. (1986). Implication of attenuation for studies of the earthquake source, in *Earthquake Source Model*, Maurice Ewing Series 6, S. Das, J. Boatwrigth, and C. H. Scholz (Editors), American Geophysical Union, Washington, D.C., 311-318.

Anderson, J. G. (1991). A preliminary descriptive model for the distance dependence of the spectral decay parameter in southern California, *Bull. Seism. Soc. Am.* **81**, 2186-2193.

Anderson, J. G., and S. E. Hough (1984). A model for the shape of the Fourier amplitude spectrum of acceleration at high frequencies, *Bull. Seism. Soc. Am.* **74**, 1969-1994.

Beresnev, I.A., and G. M. Atkinson (1997). Modeling finite-fault radiation from the ω^n spectrum, *Bull. Seism. Soc. Am.* **87**, 67-84.

Bindi, D., S. Parolai, H. Grosser, C. Milkereit, and S. Zünbul (2006). Cumulative attenuation along source-to-receiver paths in Northwestern Turkey, *Bull. Seism. Soc. Am.* **96**, 188-199.

Boatwright, J. (1978). Detailed analysis of two small New York State earthquake sequences, *Bull. Seism. Soc. Am.* **68**, 1117-1131.

Boore, D., and G. Atkinson (1987). Stochastic prediction of ground motion and spectral response parameters at hard-rock sites in eastern North America, *Bull. Seism. Soc. Am.* **77**, 440-867.

Brancato, A., J. A. Hole, S. Gresta, and J. N. Beale (2009). Determination of seismogenic structures in Southeastern Sicily (Italy) by high-precision relative re location of microearthquakes, *Bull. seism. Soc. Am.* **99**, 1921-1936.

Brune, J. N. (1970). Tectonic stress and the spectra of seismic shear waves for earthquakes, *J. Geophys. Res*. **75**, 4997-5009.

Brune, J. N. (1971). Correction, *J. Geophys. Res.* **76,** 5002.

Castro, R. R., L. Troiani, G. Monachesi, M. Mucciarelli, and M. Cattaneo (2000). The spectral decay parameter κ in the region of Umbria-Marche, Italy, *J. Geophys. Res*. **105**, 23.811-23.823.

Frémont, M. J., and S. D. Malone (1987). High precision relative locations of earthquakes at Mount St. Helens, Washington, *J. Geophys. Res*. **92**, 10.223-10.236.

Frepoli, A., and A. Amato (2000). Fault plane solutions of crustal earthquakes in Southern Italy (1988-1995): seismotectonic implications, *Ann. Geofis*. **43**, 437-467.

Giardini D., B. Palombo, and N. A. Pino (1995). Long period modelling of MEDNET waveforms for the December 13, 1990 eastern Sicily earthquake, *Ann. Geofis.* **38**, 267-282.

Halldorsson, B., and A. S. Papageorgiou (2005). Calibration of the specific barrier model to earthquakes of different tectonic regions, *Bull. seism. Soc. Am.* **95**, 1276-1300.

Iwata, T., and K. Irikura (1988). Source parameters of the 1983 Japan Sea earthquake sequence, *J. Phys. Earth*. **36**, 155-184.

Lahr, J.C. (1999). HYPOELLIPSE/VERSION 1.0: A computer program for determining local earthquake hypocentral parameters, magnitude and first motion pattern, (Y2K compliant version), *U.S. Geol. Surv. Open-File Rept. 99/23*, 99 pp.

Lawson, C. L., and R. J. Hanson (1974). Solving least squares problems, Prentice-Hall, Inc., Englewood Cliffs, New Jersey.

Musumeci, C., G. Di Grazia, and S. Gresta (2003). Minimum 1-D velocity model in Southeastern Sicily (Italy) from local earthquake data: an improvement in location accuracy, *J. Seismol*, **7**, 469-478.

Parolai, S., D. Bindi, E. Durukal, H. Grosser, and C. Milkereit (2007). Source parameters and seismic moment-magnitude scaling for northwestern Turkey, *Bull. Seism. Soc. Am*. **97**, 655-660.

Petukhin, A., and K. Irikura (2000). A method for the separation of source and site effects and the apparent Q structure from strong motion data, *Geophys. Res. Lett.* **27**, 3429-3432.

Purvance, M.D., and J. G. Anderson (2003). A comprehensive study of the observed spectral decay in strong- motion accelerations recorded in Guerrero, Mexico, *Bull. Seism. Soc. Am*. **93**, 600-611.

Reasenberg, P.A., and D. Oppenheimer (1985). Fortran computer programs for calculating and displaying earthquake fault-plane solutions, *U.S. Geol. Surv. Open-File Rept. 85-379*, 109 pp.

Safak, E. (1995). Discrete time analysis of seismic site amplification, *J. Eng. Mech. ASCE* **121,** 801–809.

Scarfì, L., H. Langer, and S. Gresta (2003). High-precision locations of two microearthquake clusters in Southeastern Sicily, Italy, *Bull. Seism. Soc. Am.* **93**, 1479-1497.

Tusa, G., A. Brancato, and S. Gresta, (2006a). Source parameters of microearthquakes at Mount St Helens (USA), *Geophys. J. Int.* **166,** 1193–1223.

Tusa, G., A. Brancato, and S. Gresta (2006b). Source parameters of microearthquakes in Southeastern Sicily, Italy, *Bull. Seism. Soc. Am.* **96**, 968–983,

Tusa, G., and S. Gresta (2008). Frequency-dependent attenuation of P waves and estimation of earthquake source parameters in Southeastern Sicily, Italy, *Bull. Seism. Soc. Am.* **98**, 2772–2794.

Tsai, C.-C. P., and K.-C. Chen (2000). A model for the high-cut process of strong-motion accelerations in terms of distance, magnitude, and site conditions: an example from the SMART 1 array, Lotung, Taiwan, *Bull. Seism. Soc. Am.* **90**, 1535-1542.

Istituto Nazionale di Geofisica e Vulcanologia – Osservatorio Etneo

Piazza Roma 2 – 95125 Catania, Italy

giuseppina.tusa@ct.ingv.it; langer@ct.ingv.it

(G.T. and H.L.)

Dipartimento di Scienze Geologiche

Università di Catania

Corso Italia 57 - 95129 Catania - Italy

abranca@unict.it; gresta@unict.it

(A. B. and S. G.)

Table 1 - Selection of source model. Min, Max, and Mean are the minimum, the maximum, and the mean values of the misfit function, respectively. The percentage change indicates the increase in the misfit function values from the Brune ω^n model.

Source model	misfit			% Change		
	Min	Max	Mean	Min	Max	Mean
Brune ω^2	0.096	0.232	0.157	0%	109%	28%
Boatwright ω^2	0.091	0.223	0.154	-2%	95%	25%
Brune ω^n	0.078	0.158	0.124	-	-	-
Boatwright ω^n	0.089	0.164	0.132	-2%	18%	6%

Table 2 - Values of the spectral decay parameter κ_{ij} for the events used in this study. Only the values with SD<100% are listed.

CL1			CL2a (Family 1)			CL2b (Family 2)			CL3		
ID	Station	κ_{ij} (sec)	ID	Station	κ_{ij} (sec)	ID	Station	κ_{ij} (sec)	ID	Station	κ_{ij} (sec)
9004	CIU	0.0366±0.0067	1	SR1	0.0153±0.0061	25	SR1	0.0187±0.0045	3	SR2	0.0468±0.0043
	MSV	0.0761±0.0087		SR3	0.0123±0.0040		SR2	0.0112±0.0073		SR3	0.0292±0.0073
9006	CIU	0.0871±0.0049		SR9	0.0034±0.0056		SR3	0.0079±0.0062		SR4	0.0712±0.0041
	CRN	0.0366±0.0062	2	SR1	0.0176±0.0058	27	SR1	0.0225±0.0049		SR7	0.0335±0.0042
	MSV	0.0590±0.0087	3	SR1	0.0258±0.0073		SR2	0.0246±0.0078		SR9	0.0242±0.0062
	TDA	0.0288±0.0045		SR2	0.0036±0.0038		SR3	0.0146±0.0040	5	SR3	0.0276±0.0081
9007	CIU	0.0649±0.0046		SR3	0.0223±0.0089	28	SR1	0.0165±0.0051		SR4	0.0519±0.0040
	MSV	0.0393±0.0070		SR5	0.0181±0.0049		SR3	0.0110±0.0062		SR5	0.0134±0.0067
	TDA	0.0427±0.0052		SR9	0.0388±0.0080	29	SR1	0.0061±0.0054		SR9	0.0290±0.0099
9009	CIU	0.0348±0.0059	5	SR1	0.0426±0.0101		SR3	0.0077±0.0063	6	SR3	0.0166±0.0080
	CRN	0.0421±0.0109		SR3	0.0242±0.0047	36	SR1	0.0173±0.0056		SR5	0.0782±0.0110
	MSV	0.0532±0.0045		SR5	0.0092±0.0039		SR2	0.0073±0.0060		SR9	0.0162±0.0069
9010	AUG	0.0248±0.0075		SR9	0.0348±0.0054		SR3	0.0017±0.0066	8	SR3	0.0276±0.0066
	CIU	0.0689±0.0051	7	SR1	0.0285±0.0071	40	SR1	0.0347±0.0044		SR9	0.0293±0.0071
	MSV	0.0537±0.0129	8	SR2	0.0054±0.0035		SR2	0.0261±0.0072	9	SR2	0.0374±0.0071
	TDA	0.0492±0.0109		SR3	0.0252±0.0067		SR3	0.0343±0.0054		SR3	0.0266±0.0045
9019	CIU	0.0478±0.0046		SR9	0.0571±0.0050	49	SR3	0.0065±0.0050		SR4	0.0343±0.0036
	MSV	0.0412±0.0061	13	SR1	0.0447±0.0042	51	SR1	0.0369±0.0059		SR9	0.0199±0.0067
	TDA	0.0291±0.0085		SR2	0.0269±0.0043		SR2	0.0135±0.0076			
				SR3	0.0203±0.0041		SR3	0.0252±0.0042			
			14	SR2	0.0070±0.0065	53	SR2	0.0106±0.0083			
				SR3	0.0161±0.0034		SR3	0.0348±0.0050			
			16	SR2	0.0156±0.0044						
				SR3	0.0043±0.0033						

Table 3 - Values of κ_i^E term for the selected events.

CL1		CL2a (Family 1)		CL2b (Family 2)		CL3	
ID	κ_i^E(sec)	ID	κ_i^E(sec)	ID	κ_i^E(sec)	ID	κ_i^E(sec)
9004	0.0178±0.0027	1	.-0.0008±0.0013	25	-	3	0.0244±0.0026
9006	0.0183±0.0014	2	-	27	0.0054±0.0022	5	0.0039±0.0018
9007	0.0106±0.0023	3	0.0105±0.0036	28	0.0001±0.0018	6	0.0111±0.0044
9009	0.0040±0.0033	5	0.0103±0.0028	29	-	8	0.0151±0.0036
9010	0.0253±0.0054	7	-	36	-	9	0.0120±0.0031
9019	0.0120±0.0030	8	0.0149±0.0021	40	0.0126±0.0016		
		13	0.0132±0.0006	49	-		
		14	-	51	0.0122±0.0017		
		16	0.0058±0.0017	53	-		

Table 4 - Values of κ_{ij}^{Diff} term for the selected events. The asterics indicate the ID of events used as reference to compute κ_{ij}^{Diff} (see text for details). Δ is the distance from the reference event.

CL1

Station	ID	κ_{ij}^{Diff}(sec)	Δ (km)
CIU	9004	-0.0120±0.0014	1.732
	9006	0.0380±0.0011	1.336
	9007	0.0234±0.0003	0.626
	9009*	0	
	9010	0.0128±0.0029	0.998
	9019	0.0049±0.0009	1.320
CRN	**9006***	0	
	9009	0.0196±0.0027	1.336
MSV	9004	0.0297±0.0013	1.681
	9006	0.0121±0.0027	1.657
	9007*	0	
	9009	0.0206±0.0035	0.626
	9010	-0.0002±0.0029	0.998
	9019	0.0006±0.0015	1.320
TDA	**9006***	0	
	9007	0.0215±0.0002	1.657
	9009	0.0133±0.0024	1.336
	9019	0.0065±0.0031	0.631

CL2a (Family 1)

Station	ID	κ_{ij}^{Diff}(sec)	Δ (km)
SR1	**1***	0	
	3	-0.0008±0.0011	0.162
	5	0.0162±0.0024	0.156
	13	0.0154±0.0012	0.443
SR2	13	0.0039±0.0010	0.079
	16*	0	
SR3	**1***	0	
	3	-0.0013±0.0026	0.162
	5	0.0008±0.0009	0.156
	8	-0.0028±0.0018	0.324
	13	-0.0060±0.0008	0.443
SR5	3	0.0087±0.0003	0.021
	5*	0	
SR9	3	0.0038±0.0019	0.021
	5*	0	
	8	0.0177±0.0003	0.164

CL2b (Family 2)

Station	ID	κ_{ij}^{Diff}(sec)	Δ (km)
SR1	27	0.0007±0.0007	0.154
	28*	0	
	40	0.0057±0.0005	0.144
	51	0.0083±0.0009	0.183
SR2	**27***	0	
	40	-0.0057±0.0001	0.042
SR3	**27***	0	
	40	0.0125±0.0019	0.042

CL3

Station	ID	κ_{ij}^{Diff}(sec)	Δ (km)
SR2	3	-0.0029±0.0023	1.276
	9*	0	
SR3	3	-0.0008±0.0011	1.404
	5	0.0182±0.0028	0.908
	6*	0	
	8	0.0070±0.0007	0.144
	9	0.0090±0.0022	0.181
SR4	3	0.0245±0.0010	1.276
	5	0.0258±0.0017	0.74
	9*	0	
SR9	3	-0.0054±0.0011	1.404
	5	0.0200±0.0056	0.908
	6*	0	
	8	0.0090±0.0010	0.144
	9	0.0027±0.0011	0.181

Table 5 - Parameters used to calcule the sinthetic spectra

Source	Half-space	Bedrock	Soft Layer
$\Delta\sigma$ = 1MPa	V = 6000 m/s	V_1 = 4000 m/s	600 m/s $\leq V_2 \leq$ 1800 m/s
R_p = 0.4	ρ = 2800 kg/m^3	ρ_1 = 2700 kg/m^3	ρ_2 = 2700 kg/m^3
1.5 $\leq M_L \leq$ 3	0.02 $\leq \kappa_h \leq$ 0.04 s		10 $\leq Q_2 \leq$ 50
			d_2 = 100 m
log M_0 = 0.99M_L + 17.6 *			

Values of the single parameters used for each simulated event				
	M_L	Q_2	b	V_2
Event 1	1.5	50	0.4	1800
Event 2	1.8	30	0.8	1500
Event 3	2.1	20	1.2	1200
Event 4	2.4	10	1.4	900
Event 5	3	10	2.0	600

* From Tusa and Gresta (2008)

Figure captions

Figure 1 – Map of the seismic networks used in this study and historical seismicity (Azzaro and Barbano, 2000). The epicentral locations of seismic sequences analyzed are also shown. The focal mechanisms of the 13 December main shock (centroid moment tensor fault-plane solution) (Giardini *et al*., 1995) and the 16 December event are also reported (Amato *et al*., 1995).

Figure 2 – First motion focal mechanisms of the events (a) of the December 1990 sequence and (b) of the February – September 2002 swarm (from Brancato *et al*., 2009).

Figure 3 – Acceleration density source spectra for all the clusters used in this study as resulting from the inversion procedure.

Figure 4 – Displacement (a) and acceleration (b) density source spectra for the event #40 belonging to the cluster CL2b. The lines indicate the best-fitting theoretical spectra for each of the four spectral models (see text for details).

Figure 5 – Examples of acceleration density spectra of P-wave corresponding to different events at the same station for (a) cluster CL1, (b) cluster CL2a, and (c) cluster CL3. Superimposed on each spectrum is a linear, least-squares fit over the investigated frequency bands (see text for details). The event ID, the station code, the value of κ_{ij}, and the local magnitude (M_L) are also indicated in each panel.

Figure 6 – (a) A plot of κ^E term (±1 standard deviation) against the local magnitude (M_L), with line indicating the least-squares fit. (b) κ^P term (±1 standard deviation) against hypocentral distance for

all four clusters of events. Dark-grey, light-grey and black symbols are associated to the stations SR2, SR3 and SR9 that are the only ones shared by three of the four clusters.

Figure 7 – Comparison between κ_{tot}, imposed by the model used to generate the synthetic spectra and κ_{totE} (estimated from the synthetic spectra). The vertical bars are the standard errors related to κ_{totE} as obtained from the regression analysis.

Figure 8 – Comparison between the input (true) and inverted (estimated) values of the κ_{event}, κ_P, and κ_{Diff} (κ_E^i, κ_P^j, and κ_{Diff}^{ij}, respectively, for the event *i* at site *j*).

Figure 9 – Plot of log of source radius (r) versus log of seismic moment (M_0). The lines are contours of equal stress-drops in bars. Open circles refer to results obtained by Tusa *et al*. (2006b) for six of the eighteen events belonging to the clusters CL2a and b. The grey lines indicate the error factor associated to estimates (see Tusa *et al*. (2006b) for details).

Supplemental Material

The electronic supplement to this article includes three Tables (Tables i, ii and iii) which captions are the following:

Table S1 - Stations of mobile seismic network used in this study.

Table S2 - Station coordinates of the SESSN.

Table S3 - Average values of $\kappa^{P}+\kappa^{Diff}$. Errors are the standard deviation of the mean.

Figure
Click here to download Figure: figures.pdf

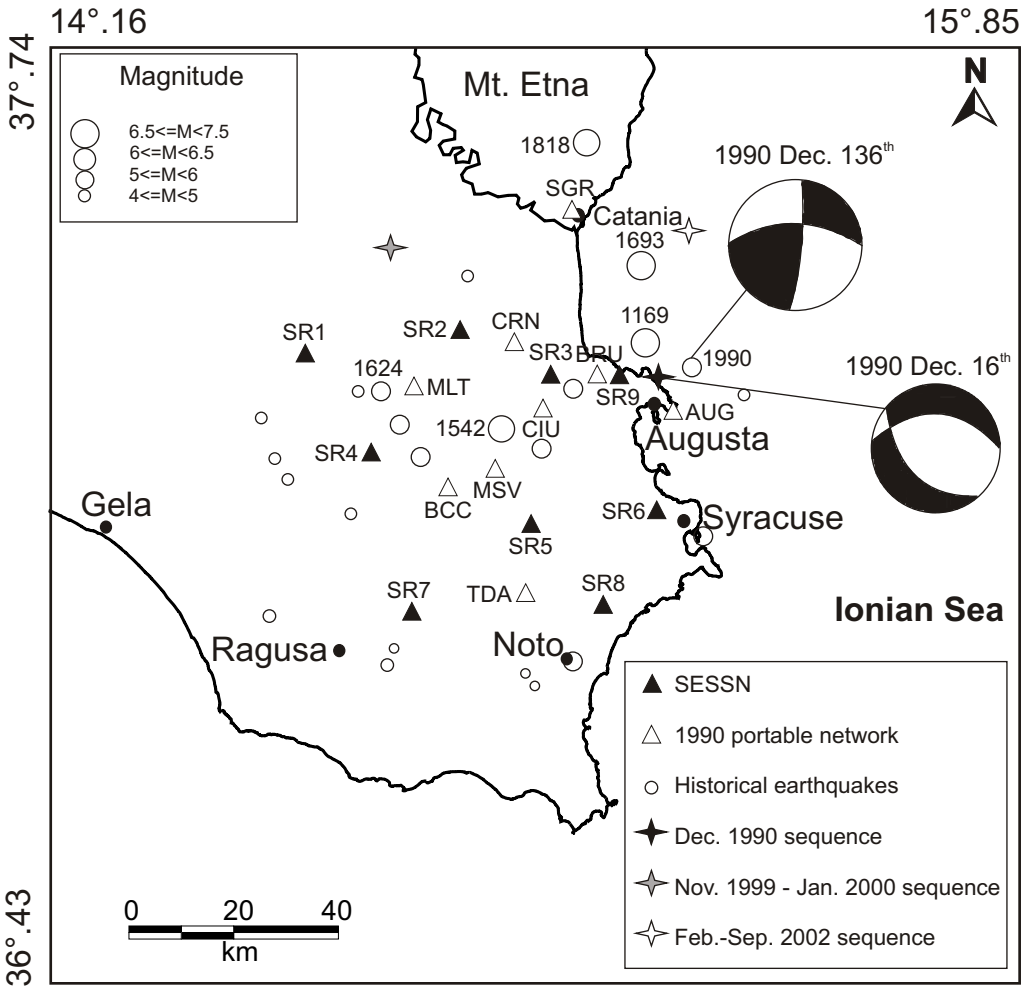

Figure 1

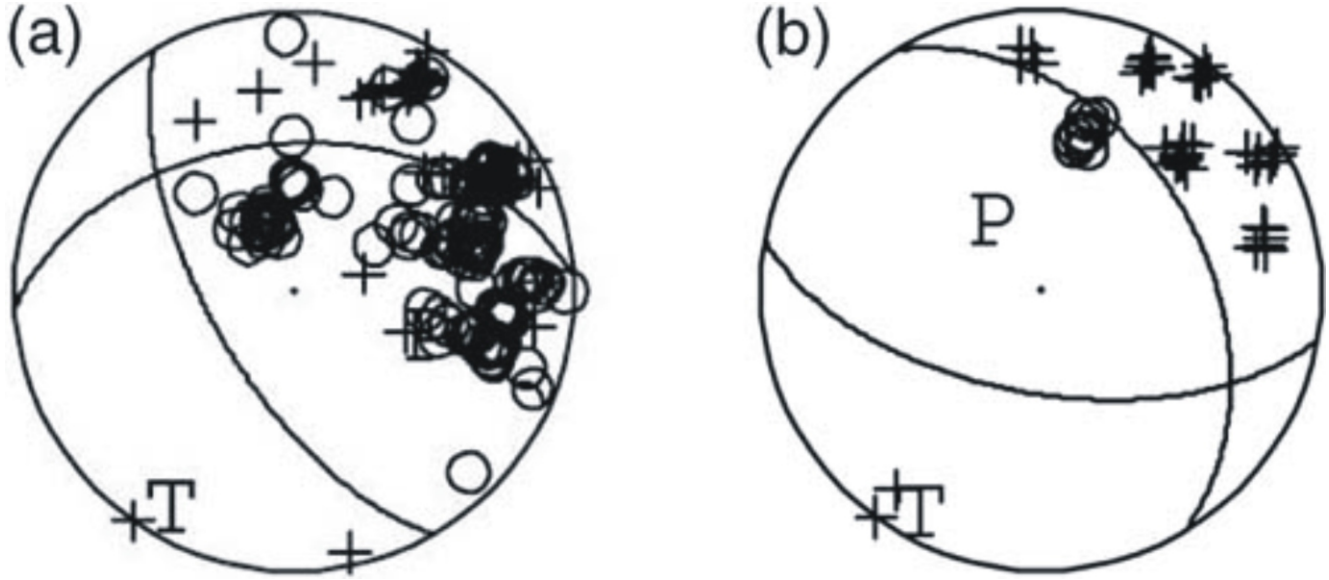

Figure 2

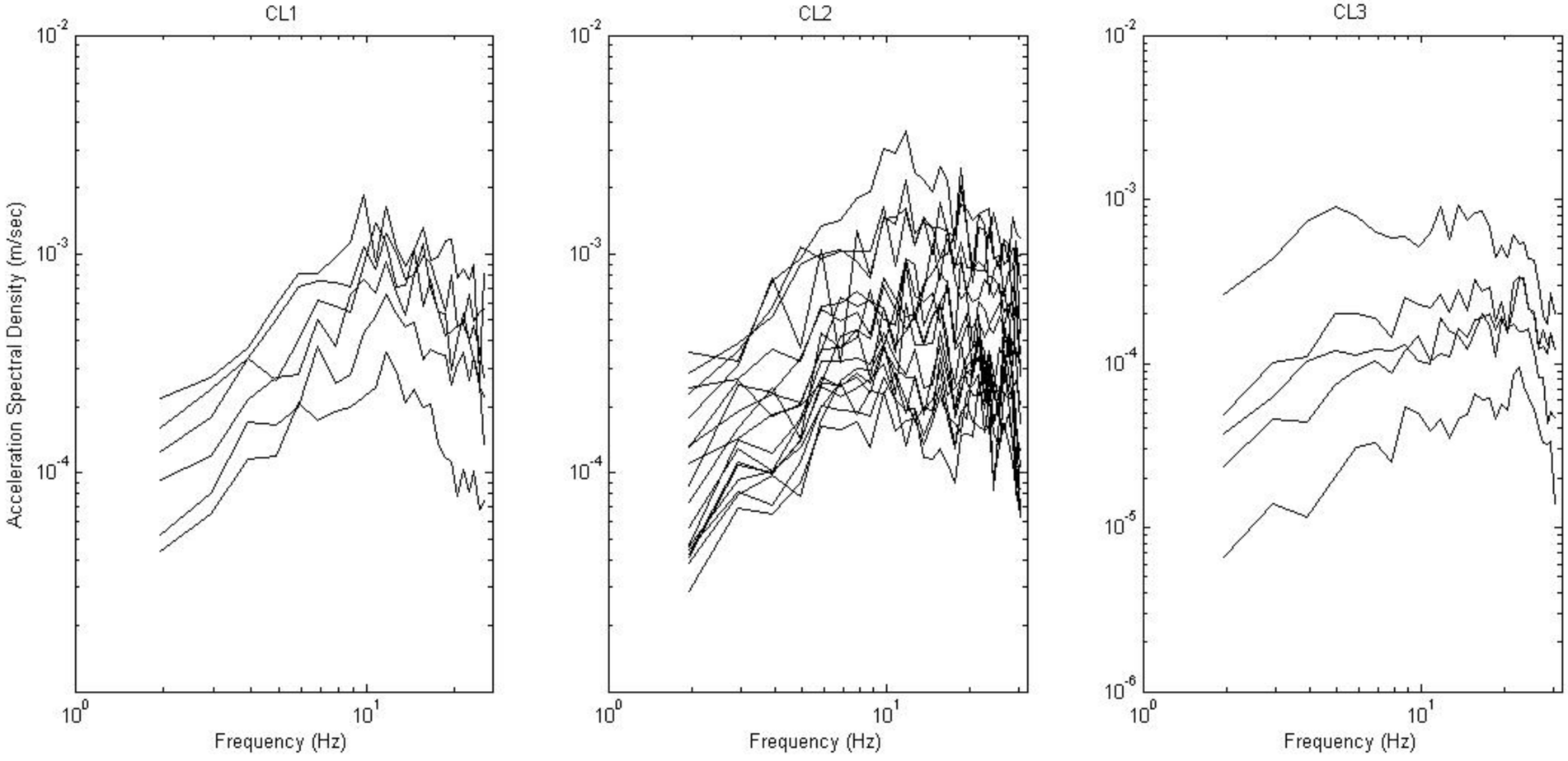
CL1
CL2
CL3
Acceleration Spectral Density (m/sec)
Frequency (Hz)
Frequency (Hz)
Frequency (Hz)

Figure 3

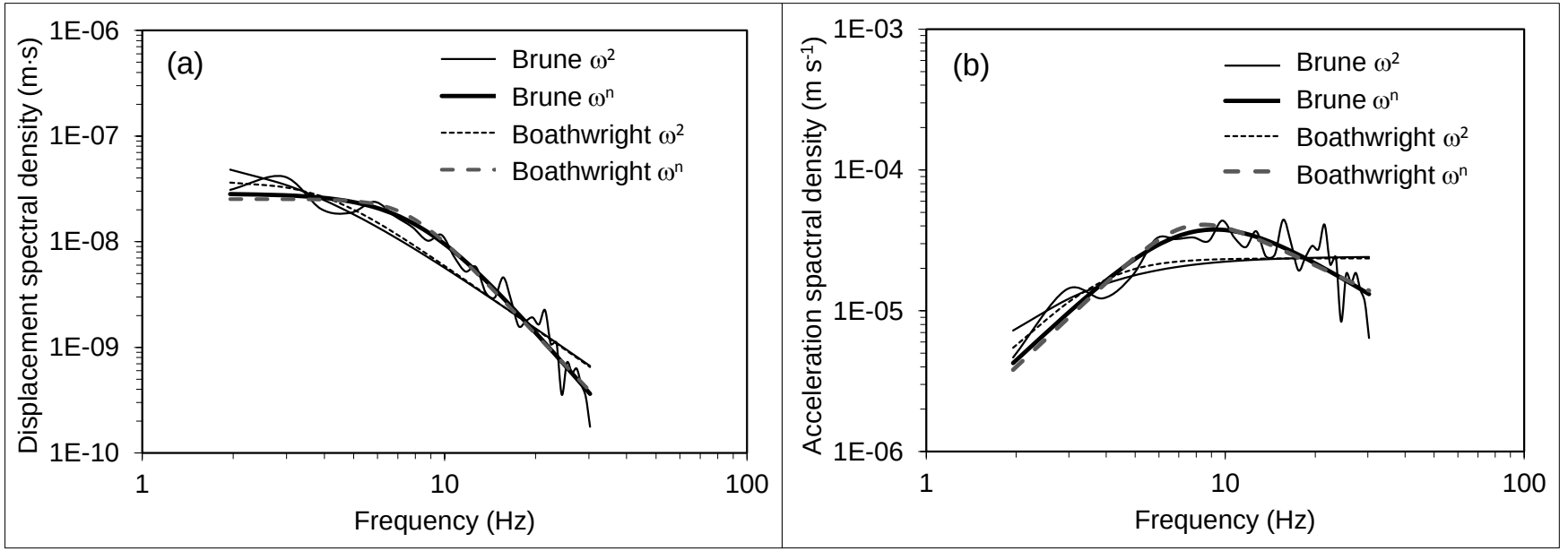
(a)
Brune ω²
Brune ωⁿ
Boathwright ω²
Boathwright ωⁿ
Displacement spectral density (m·s)
1E-06
1E-07
1E-08
1E-09
1E-10
1
10
100
Frequency (Hz)
(b)
Brune ω²
Brune ωⁿ
Boathwright ω²
Boathwright ωⁿ
Acceleration spactral density (m s⁻¹)
1E-03
1E-04
1E-05
1E-06
1
10
100
Frequency (Hz)

Figure 4

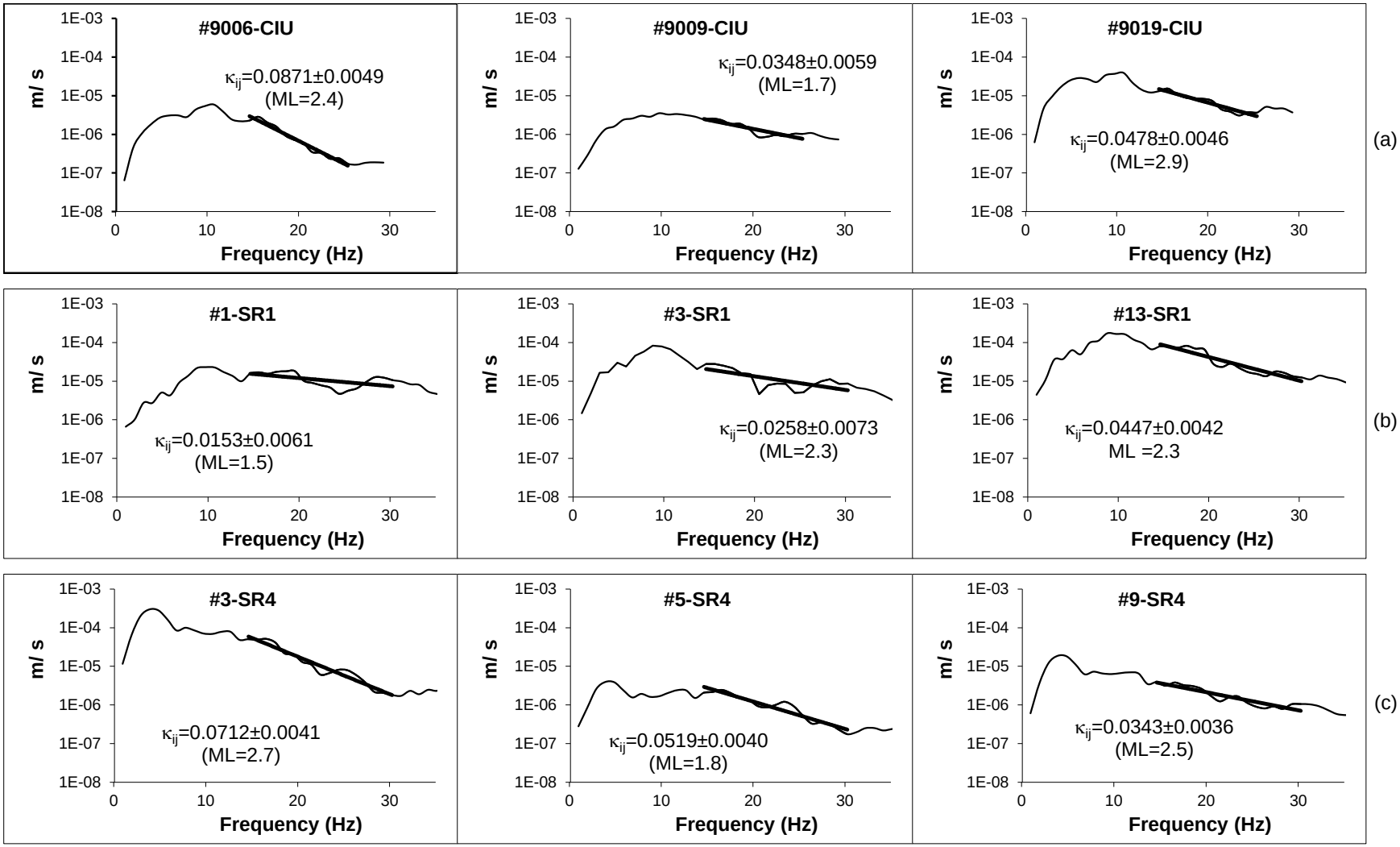
#9006-CIU
κij=0.0871±0.0049
(ML=2.4)
#9009-CIU
κij=0.0348±0.0059
(ML=1.7)
#9019-CIU
κij=0.0478±0.0046
(ML=2.9)
(a)
#1-SR1
κij=0.0153±0.0061
(ML=1.5)
#3-SR1
κij=0.0258±0.0073
(ML=2.3)
#13-SR1
κij=0.0447±0.0042
ML =2.3
(b)
#3-SR4
κij=0.0712±0.0041
(ML=2.7)
#5-SR4
κij=0.0519±0.0040
(ML=1.8)
#9-SR4
κij=0.0343±0.0036
(ML=2.5)
(c)
m/ s
Frequency (Hz)
1E-03
1E-04
1E-05
1E-06
1E-07
1E-08
0
10
20
30

Figure 5

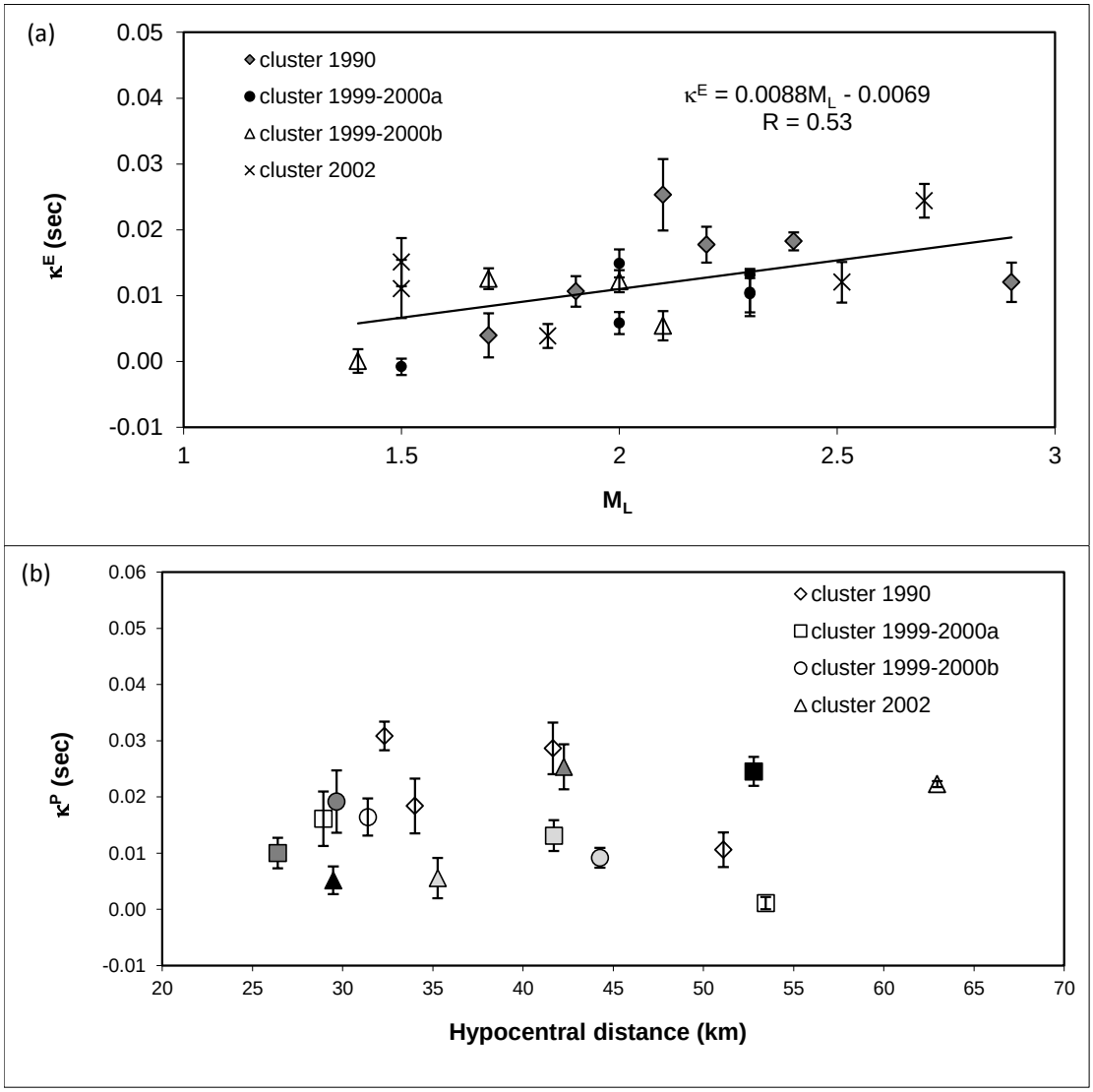
(a)
cluster 1990
cluster 1999-2000a
cluster 1999-2000b
cluster 2002
$\kappa^E = 0.0088M_L - 0.0069$
R = 0.53
κ^E (sec)
M_L
(b)
cluster 1990
cluster 1999-2000a
cluster 1999-2000b
cluster 2002
κ^P (sec)
Hypocentral distance (km)

Figure 6

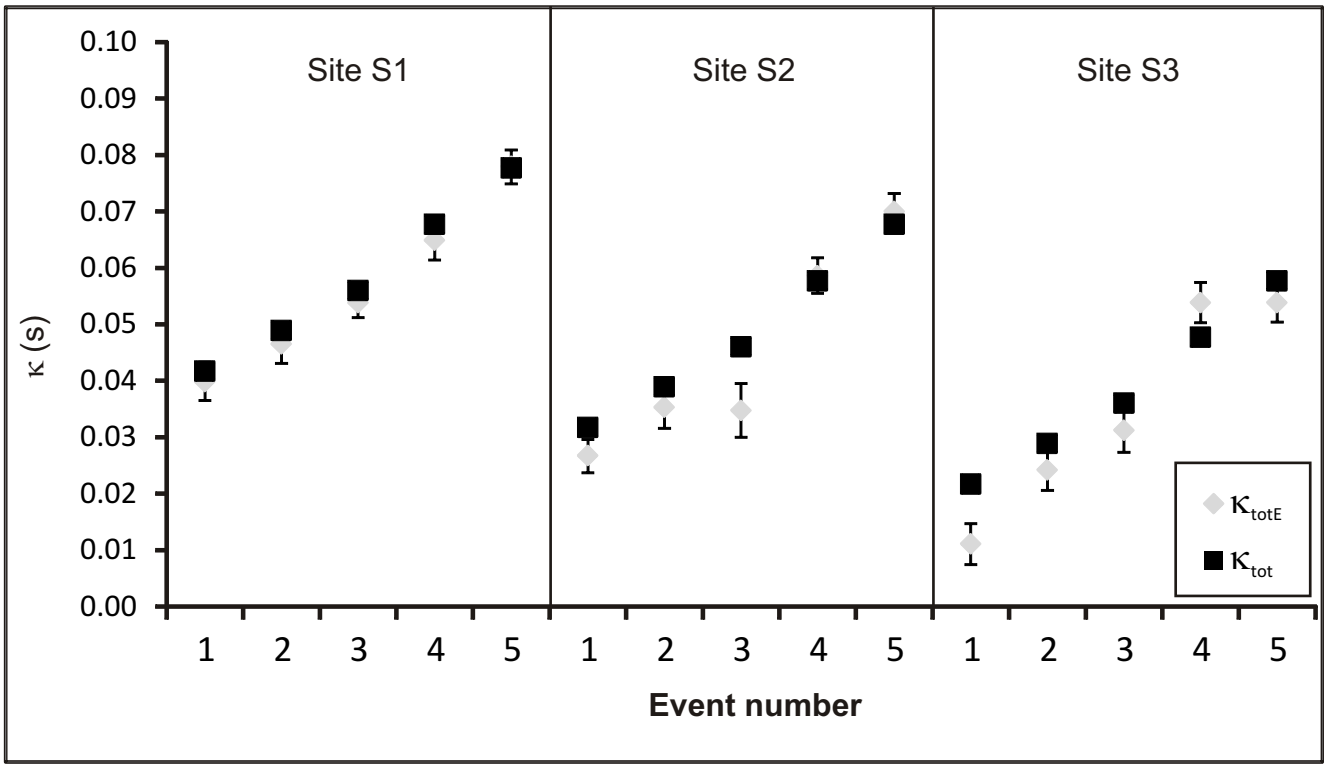
Site S1
Site S2
Site S3
κ (s)
0.10
0.09
0.08
0.07
0.06
0.05
0.04
0.03
0.02
0.01
0.00
1 2 3 4 5 1 2 3 4 5 1 2 3 4 5
Event number
κtotE
κtot

Figure 7

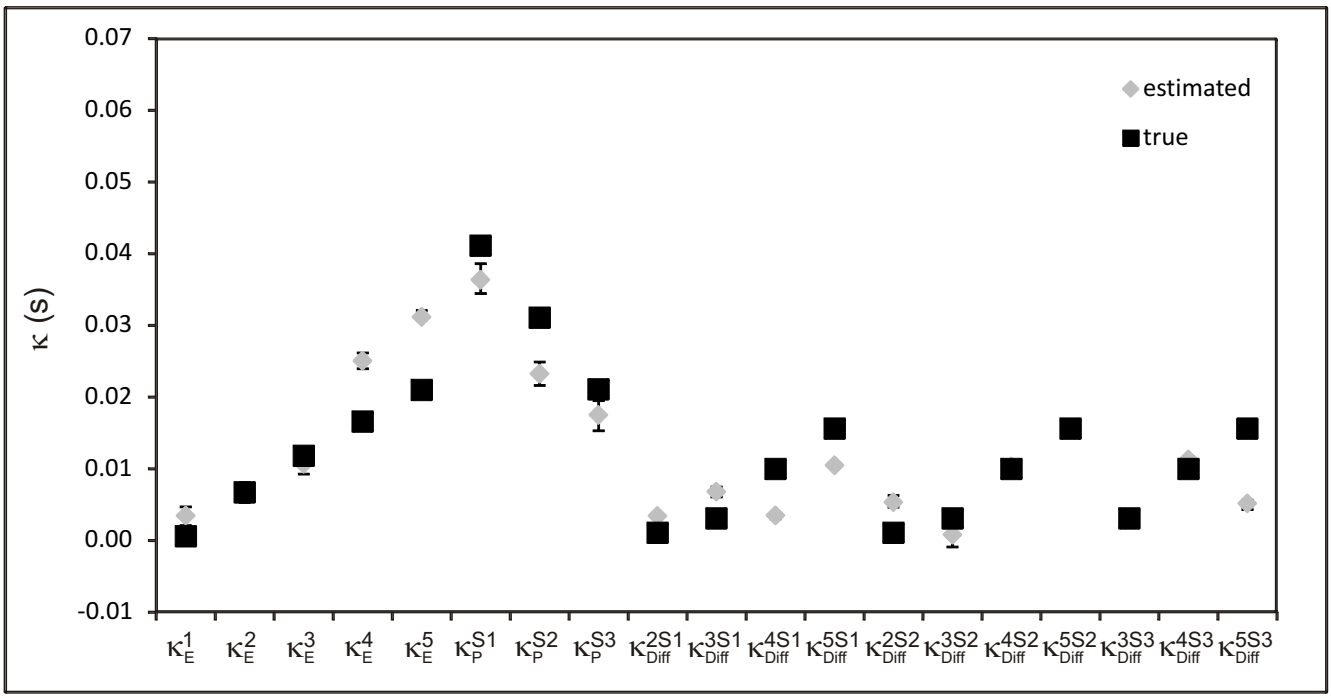
0.07
0.06
0.05
0.04
0.03
0.02
0.01
0.00
-0.01
κ (s)
estimated
true
κ_E^1 κ_E^2 κ_E^3 κ_E^4 κ_E^5 κ_P^{S1} κ_P^{S2} κ_P^{S3} κ_{Diff}^{2S1} κ_{Diff}^{3S1} κ_{Diff}^{4S1} κ_{Diff}^{5S1} κ_{Diff}^{2S2} κ_{Diff}^{3S2} κ_{Diff}^{4S2} κ_{Diff}^{5S2} κ_{Diff}^{3S3} κ_{Diff}^{4S3} κ_{Diff}^{5S3}

Figure 8

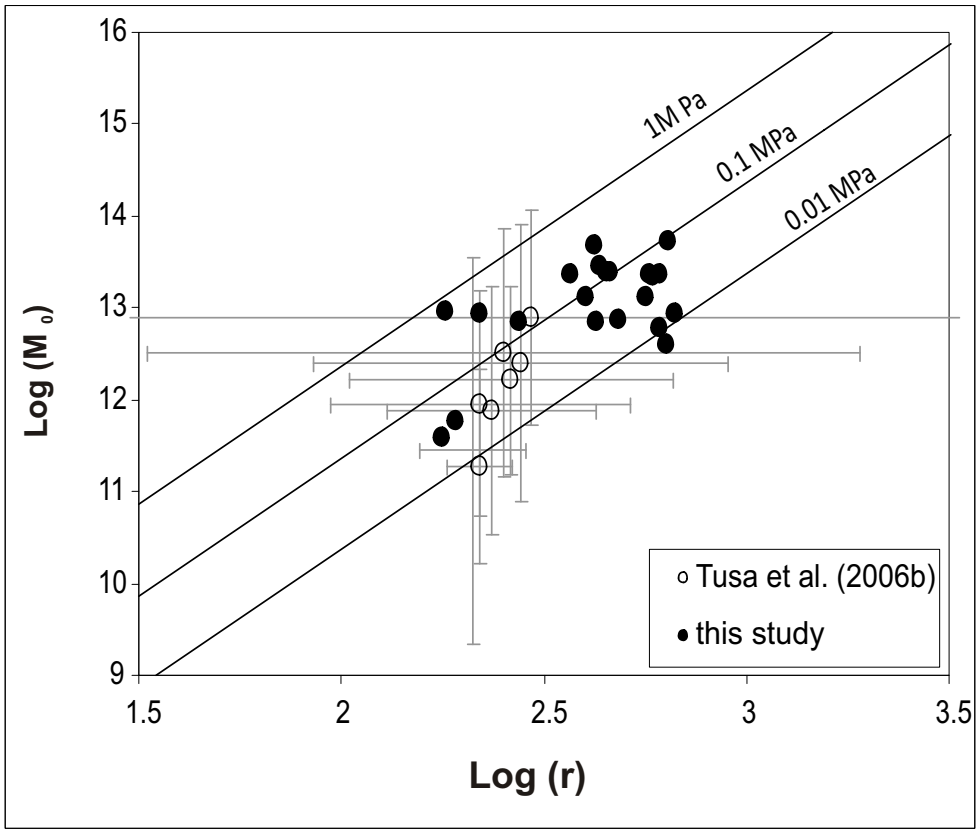
16
15
14
13
12
11
10
9
1.5
2
2.5
3
3.5
Log (M o)
Log (r)
1M Pa
0.1 MPa
0.01 MPa
Tusa et al. (2006b)
this study

Figure 9

Supplemental Material

Click here to download Supplemental Material: SupplementalMaterial.htm